PCCP

PAPER

View Article Online
View Journal | View Issue

Cite this: *Phys. Chem. Chem. Phys.*, 2017, **19**, 19822

XUV-induced reactions in benzene on sub-10 fs timescale: nonadiabatic relaxation and proton migration

M. C. E. Galbraith,[a] C. T. L. Smeenk,[a] G. Reitsma,[a] A. Marciniak,[b] V. Despré,[b] J. Mikosch,[a] N. Zhavoronkov,[a] M. J. J. Vrakking,[a] O. Kornilov *[a] and F. Lépine[b]

Received 7th April 2017,
Accepted 15th June 2017

DOI: 10.1039/c7cp02255g

rsc.li/pccp

Unraveling ultrafast dynamical processes in highly excited molecular species has an impact on our understanding of chemical processes such as combustion or the chemical composition of molecular clouds in the universe. In this article we use short (<7 fs) XUV pulses to produce excited cationic states of benzene molecules and probe their dynamics using few-cycle VIS/NIR laser pulses. The excited states produced by the XUV pulses lie in an especially complex spectral region where multi-electronic effects play a dominant role. We show that very fast $\tau \approx 20$ fs nonadiabatic processes dominate the relaxation of these states, in agreement with the timescale expected for most excited cationic states in benzene. In the CH_3^+ fragmentation channel of the doubly ionized benzene cation we identify pathways that involve structural rearrangement and proton migration to a specific carbon atom. Further, we observe non-trivial transient behavior in this fragment channel, which can be interpreted either in terms of propagation of the nuclear wavepacket in the initially excited electronic state of the cation or as a two-step electronic relaxation *via* an intermediate state.

1 Introduction

Excited radical species often play a key role in important chemical processes. In combustion they define intermediate steps leading to exoenergetic reactions and therefore determine the efficiency of the overall process and its energy balance.[1] In interstellar medium they are the most abundant chemical forms for both small and large molecules. Understanding their physical properties and reactivity is crucial for the assignment of emission and absorption spectra measured by telescopes and for the chemical fate of the interstellar medium in terms of molecular complexity.[2]

Gas phase radicals, in particular radical ions, have been thoroughly investigated at synchrotrons and in low energy collision experiments. In these experiments the excitation step is sufficient to produce radicals with high internal energy and to observe fragmentation or ionisation, but with no means to disentangle the intermediate "transition" states and reaction paths leading to specific photoproducts. Consequently, very limited insight is obtained on ultrafast processes following the initial excitation step, which may bear strong multi-electronic character[3] and can initiate ultrafast non-radiative decay[4] or major structural rearrangements involving ultrafast proton motion.[5] Insights into this ultrafast regime have become possible with the use of short laser pulses, which give access to time-resolved investigations of reactions following the excitation of low-lying electronic molecular states. Ultrafast isomerisation, nonadiabatic relaxation and charge transfer were investigated using time-resolved mass spectrometry, absorption and photo-electron spectroscopy.[6,7]

The recent development of novel ultrafast sources in the XUV range allows us to apply the methods of femtochemistry to study the dynamics of highly excited radicals. Ultrashort XUV pulses combining high photon energy and short pulse duration allow the time-resolved inspection of highly excited species and offer new means to investigate systems, where electron correlation and non-Born–Oppenheimer dynamics are essential to understand the photo-induced mechanisms. So far XUV-induced ultrafast processes have been revealed in a limited number of experiments on small molecular species. Multi-electronic states have been excited in N_2, O_2 and NO_2 by XUV pulses and their subsequent dynamics have been followed.[8–11] These experiments have been only recently extended to larger molecules. Few femtosecond oscillations of the yield of selected fragmentation products were observed in phenylalanine[12] and multi-electronic excitation followed by nonadiabatic relaxation of polycyclic aromatic hydrocarbons (PAHs) could be studied for naphthalene, anthracene, pyrene and tetracene molecules.[13]

[a] *Max-Born-Institut, Max-Born-Straße 2A, 12489 Berlin, Germany. E-mail: kornilov@mbi-berlin.de*
[b] *Institut Lumière Matière, Université Lyon 1, CNRS, UMR 5306, 10 rue Ada Byron, 69622 Villeurbanne Cedex, France*

In this article we employ sub-10 fs XUV and VIS/NIR pulses to investigate XUV-induced relaxation mechanisms in the benzene molecule. Benzene is known to undergo extremely fast internal conversion when excited to low electronic states,[14] but little is known about the relaxation of high-lying excited states, which leads to efficient fragmentation of the molecules. So far no experiments have addressed their dynamics at ultrashort time scales and modern theoretical methods are also not yet sufficient to capture these ultrafast processes. In our experiment XUV pulses produce highly excited benzene cations which undergo ultrafast nonadiabatic relaxation. We probe the relaxation processes using a delayed VIS/NIR pulse to doubly ionise the molecules and detect the dication and its fragments using a time-of-flight spectrometer. The results allow us to identify excited states responsible for the decay mechanisms observed and to determine the relaxation rates in different channels including those leading to unimolecular dissociation.

2 Experimental

The experimental setup for XUV-NIR pump–probe spectroscopy has already been described elsewhere.[13,15] In brief, 25 fs duration NIR pulses from a 1 kHz Ti:Sa amplifier are focused into a Ne-filled static hollow-core fibre, which together with a set of dispersive mirrors is used to reduce the pulse duration from 25 fs to 7 fs and delivers a pulse energy of $\approx$1 mJ. The resulting pulses are characterised by means of spectral phase interferometry for direct electric-field reconstruction (SPIDER), *cf.* Fig. 1(a), and consistently demonstrate a duration of 7.4 fs FWHM. After the fibre the VIS/NIR beam is split into a pump and probe arm with the ratio of 70% to 30%. The pump beam is focused into a gas cell containing Xe or Ar gas thereby producing XUV light by means of high-order harmonic generation (HHG). Afterwards the VIS/NIR beam is blocked by a 200 nm foil made of Al or Sn. The use of different gases and foil materials allows for tuning of the XUV spectrum. Examples of typical HH spectra are displayed in Fig. 1(b). The Al filter transmits high photon energies and leads to a spectrum encompassing approximately 16–50 eV for high harmonics generated in Ar gas and 16–38 eV for high harmonics generated in Xe gas. The Sn filter restricts the XUV photon energies to the range 16 eV $< \hbar\omega <$ 24 eV. The pump XUV beam is recombined with the VIS/NIR probe beam using a cored mirror. The two collinear beams are then focused by a toroidal mirror into the center of a velocity map imaging spectrometer (VMIS) operated in time-of-flight (TOF) mode.[16] Benzene is injected into the VMIS through a continuous source integrated in the repeller plate.[17] The source is heated to approximately 70 °C to avoid condensation inside the nozzle and to minimise the probability of cluster creation. The cross-correlation between the XUV and the VIS/NIR beam is determined from the experimental data and amounts to 10 $\pm$ 1 fs.

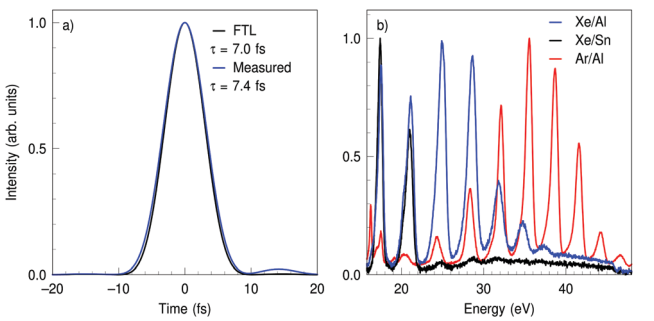

Fig. 1 (a) Characterisation of the VIS/NIR pulse using a SPIDER measurement. The black curve represents the temporal reconstruction for a Fourier transform limited pulse (FTL), and the blue curve for the actual measured pulse. (b) Examples of HHG spectra recorded with Ar and Xe gas and filtered with either Al or Sn foils.

3 Results

An ion time-of-flight (TOF) spectrum resulting from the ionisation of benzene molecules by the XUV pulses is shown in Fig. 2(a) as a black line with the time axis converted to a m/z axis. The spectrum is recorded with high harmonics (HH) generated in Ar and filtered by an Al foil, *i.e.* with the largest XUV bandwidth used in the present experiments. In this measurement the VIS/NIR pulse is not blocked, but passes through the sample 50 fs before the XUV pulse (*i.e.* at negative time delay). Owing to the low intensity ($<10^{13}$ W cm^{-2}) used in the present experiments the VIS/NIR pulse has no effect on the ground state benzene molecules. The mass peaks in the spectrum of Fig. 2 are fully resolved for m/z ratios up to at least m/z = 60. Illuminating benzene with photon energies above 14 eV leads to dissociation.[18–20] The fragmentation mechanisms are considered to be dominated by statistical pathways described by unimolecular reaction rates. With the broadest XUV bandwidth used in the experiment 17 fragments can be observed originating from dissociation of $C_6H_6^+$. XUV-only double ionisation is negligible under the conditions of the present experiment.[21,22] To address specifically the relaxation dynamics of cations in high electronically excited states this article focuses on photoproducts

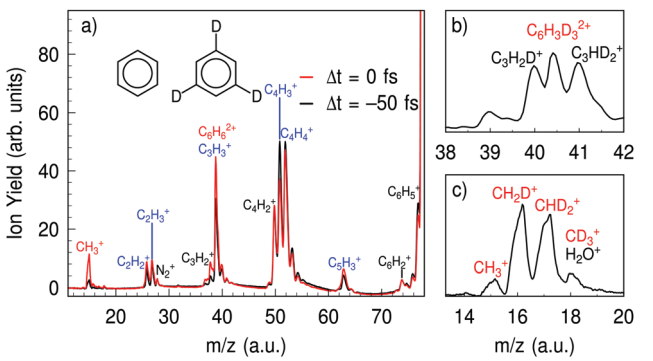

Fig. 2 (a) Ion fragment mass spectrum of C_6H_6 recorded with Ar HH and Al foil. The XUV-only spectrum (black line) is recorded by sending the VIS/NIR pulse before the XUV pulse (see text). The two-colour spectrum (red line) is recorded when the XUV and VIS/NIR pulses overlap in time. The fragments labeled in black originate from $C_6H_6^+$, the ones in red from $C_6H_6^{2+}$ and the ones in blue can be produced by fragmentation of both $C_6H_6^+$ and $C_6H_6^{2+}$ (see ref. 18). (b) Close-up view for the $C_3H_XD_{3-X}^+$/$C_6H_3D_3^{2+}$ fragment group. (c) Close-up view for the $CH_XD_{3-X}^+$ fragment group.

originating from $C_6H_6^{2+}$ ions, which are created *via* further ionisation of $C_6H_6^{+}$ by the probe VIS/NIR pulses. These ions are the $C_6H_6^{2+}$ parent ions at m/z = 39 (IP = 24.9 eV[21]) and CH_3^{+} ions at m/z = 15, which are exclusively created by fragmentation of $C_6H_6^{2+}$ and have an appearance energy AE = 27.8 eV.[18,19] High XUV photon energies lead to additional dissociation products of $C_6H_6^{2+}$, but all m/z peaks corresponding to these fragments also have contributions from dissociation of $C_6H_6^{+}$ ions (labeled blue in Fig. 2(a))[18] and are therefore much more difficult to analyse. For the doubly charged ion $C_6H_6^{2+}$, the m/z = 39 ratio is identical to that of the fragment $C_3H_3^{+}$. In order to disentangle the dynamics from these fragments, experiments with partially deuterated benzene $C_6H_3D_3$ were carried out (*cf.* sketch in Fig. 2(a)). Fig. 2(b) shows that in this case the doubly charged ion $C_6H_3D_3^{2+}$ (m/z = 40.5 a.u.) is well separated from the neighboring fragments (m/z = 40 and m/z = 41 a.u.). In the partially deuterated $C_6H_3D_3$ the $CH_XD_{3-X}^{+}$ fragmentation channel leads to all four conceivable mass peaks (Fig. 2(c)).

When the probe pulse overlaps in time with the XUV pulse, two-colour effects are best visible for the $C_6H_6^{2+}$, CH_3^{+} and $C_4H_3^{+}$ fragments (*cf.* red line in Fig. 2(a)). The ion yields of the two former fragments are increased showing an enhanced production in the presence of the VIS/NIR pulse. This observation confirms that at zero pump–probe delay the VIS/NIR pulse leads to further ionisation of the electronically excited cations. By contrast, the fragment yield of $C_4H_3^{+}$ is depleted by the VIS/NIR pulse.

A pump–probe trace of $C_6H_6^{2+}$ recorded with an approximate bandwidth of 16–50 eV (Ar HH and Al foil) is depicted in Fig. 3(a). Positive delays imply that the VIS/NIR pulse arrives at the sample after the XUV pulse. The main observation is an increase in yield around time overlap followed by a decay on the few fs-timescale. In addition, a long-lived component is visible that shows no decay within the time frame investigated. The data in Fig. 3(a) can be fit by the convolution of a Gaussian, representing the XUV-VIS/NIR cross-correlation of the experiment, with an exponential decay and a step function $\Theta(t)$. The least-squares fit leads to an ultrashort decay time of τ = 17 ± 2 fs. For the $C_6D_3H_3^{2+}$ fragment the issue of overlapping with other fragments is strongly alleviated. A measurement recorded with a bandwidth of 16–24 eV (Sn filter) for partially deuterated benzene is shown in Fig. 3(b). The long-lived component is not observed in this case. The fragments at neighboring masses m/z = 40 and 41 a.u. do not show any clear femtosecond dynamics, but do show a considerable long-lived contribution. Therefore we attribute the long-lived component visible in Fig. 3(a) to contributions from $C_3H_3^{+}$ fragments. The dependence of the decay time on variation of the XUV bandwidth and on deuteration was experimentally explored by exchanging the HH gas and the metal filters. The retrieved decay times show no significant difference between the benzene and the partially deuterated benzene; however a subtle variation of the decay time in the range of 12 to 20 fs is observed depending on the XUV bandwidth. The transients recorded with a bandwidth of 16–24 eV (Xe HH, Sn filter) appear to result in slightly faster decay times than those acquired with the bandwidth of 16–50 eV. Note that for the photon energy range of 12–16 eV two-colour effects are absent in the dication signals.[15]

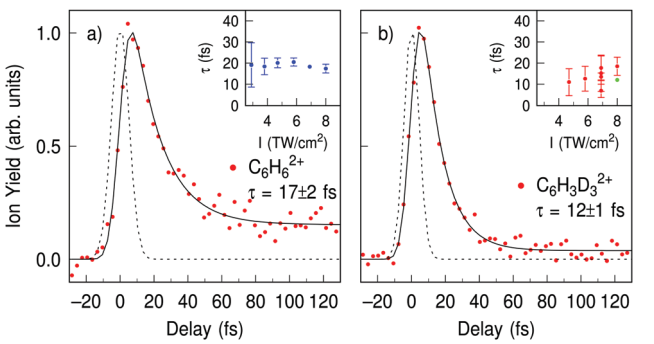

Fig. 3 Pump–probe traces of the dication: (a) transient for $C_6H_6^{2+}$ and (b) for $C_6D_3H_3^{2+}$ recorded with Ar HH/Al foil and Xe HH/Sn foil, respectively. The bold line is a fit to the data, and the dashed line represents the cross-correlation function obtained from the fit. The insets display lifetimes extracted for measurements with different VIS/NIR probe intensities.

In the experiments we vary the probe intensity to differentiate excited cationic states that require a different number of VIS/NIR photons for the second ionisation step. The probe intensity is varied by about half an order of magnitude, yet always set below 1.0×10^{13} W cm^{-2}. The insets in Fig. 3(a) and (b) display the extracted decay times for different VIS/NIR probe intensities. Changing the intensity does not lead to a measurable change in the decay time, which suggests that the same group of electronic states is probed throughout the experiment. Overall the mean decay time extracted from the measurements for the doubly charged ion is $\tau(C_6H_6^{2+})$ = 16 ± 4 fs.

The yield of the fragment CH_3^{+} also increases around XUV-VIS/NIR time overlap followed by an ultrafast decay as shown in Fig. 4(a). In this case it is found that a fit with a single exponential decay (convoluted with the XUV-VIS/NIR cross-correlation) does not lead to satisfactory agreement with the data (*cf.* bold red line in Fig. 4(a)). A significant discrepancy between the decay times obtained with the XUV-VIS/NIR cross-correlation fixed to its known 10 fs value and those obtained with the XUV-VIS/NIR cross-correlation varied as a free parameter (see Fig. 4(b)) further indicates that this model is not appropriate for the data. Consequently, two alternative fit models are applied both leading to a good agreement with the experimental data. The first approach is analogous to that taken by Suzuki *et al.* for describing internal conversion in neutral excited benzene.[23] It is assumed that the intermediate state population does not start decaying instantaneously, but that instead the exponential decay begins after a time delay Δt (implemented as a fit parameter). During the specified time the molecules remain in the initially excited state. This model is sketched in the inset of Fig. 4(a). The agreement between the measured data and the fit (bold blue line in Fig. 4(a)) is significantly better than for the single exponential decay, resulting in the smaller error bars on the fit parameters as shown in part (c) of the figure. Contrary to the case of a single exponential decay, allowing the XUV-VIS/NIR cross-correlation to be varied as a fit parameter does not change the quality of the fit, further supporting the validity of this approach. This is shown by the red (free cross-correlation) and blue (fixed cross-correlation) dots in Fig. 4(c). The extracted relaxation time for

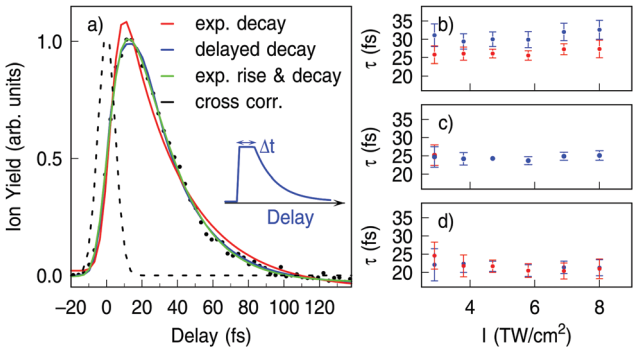

Fig. 4 (a) Pump–probe trace of the fragment CH_3^+ recorded with Ar HH and Al foil. The bold red line is a single exponential fit to the data. The bold blue line represents a fit with the exponential decay delayed with respect to time "zero". This model is sketched in the inset of (a). The bold green line corresponds to the exponential rise–decay model described in the text. The dependence of the extracted lifetimes on the VIS/NIR peak intensity is summarised in (b) for the exponential, (c) for the delayed exponential and (d) for the rise–decay exponential fits. The blue dots are the fit results using the fixed cross-correlation extracted from the $C_6H_6^{2+}$ dication, whereas the red dots originate from fits where the cross-correlation is included in the fit as a free parameter.

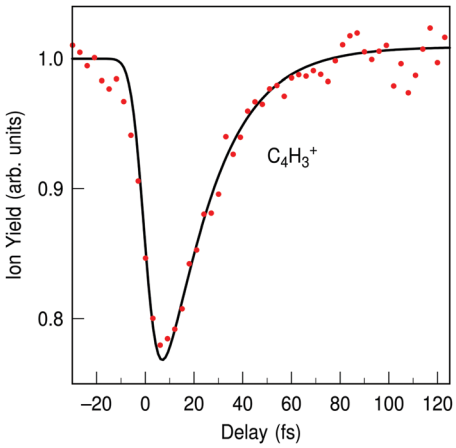

Fig. 5 Pump–probe trace of the $C_4H_3^+$ fragment recorded under the same experimental conditions as the data of Fig. 3(a) and 4 (red dots). The black curve is the sum of the single exponential decay fit to the $C_6H_6^{2+}$ data and the rise–decay fit to the CH_3^+ data with relative magnitudes adjusted for the best match to the data points. The curve is inverted to represent the depletion observed for this fragment.

the delayed exponential decay is found to be $\tau(CH_3^+) = 23 \pm 2$ fs with a delay Δt of 15 ± 7 fs.

The second model is based on a two-exponential (rise–decay) function $f(t) = A\cdot(e^{-t/\tau} - e^{-t/\Delta t})$, where A corresponds to the amplitude of the transient, τ is the decay time and Δt is now a rise time. The resulting fit is shown as a bold green line in Fig. 4(a). The agreement of the fit with the data points is evidently superior to the single exponential decay and leads to a slightly better agreement than the delayed exponential fit. For the rise–decay function a decay time of $\tau(CH_3^+) = 21 \pm 3$ fs accompanied by a rise time of $\Delta t = 7 \pm 2$ fs is determined. Within the error bars the lifetime extracted from the two-exponential (rise–decay) fit agrees with the lifetime extracted from the delayed exponential model. Note that for deuterated benzene all four $CH_xD_{3-x}^+$ fragments exhibit identical pump–probe behaviour, albeit with slightly varying signal-to-noise levels. The lifetimes observed are not significantly affected by the deuteration.

The pump–probe trace for the last fragment significantly affected by the VIS/NIR pulse, the $C_4H_3^+$ ion, is shown in Fig. 5. The data are extracted from the same experimental run as the data shown in Fig. 3(a) and 4. The time-dependent trace of the $C_4H_3^+$ fragment and the magnitude of its depletion are similar to the transients of the $C_6H_6^{2+}$ and CH_3^+ fragments. This suggests that the signal observed in this channel may correlate with the population of cationic states depleted by further ionisation with the probe VIS/NIR pulse. To test this assertion we construct a model function by summing the single exponential decay curve representing the time-dependent $C_6H_6^{2+}$ ion signal and the rise–decay curve representing the time-dependent CH_3^+ ion signal and convolute it with the Gaussian cross-correlation. Adjusting the relative weights of the two contributions to account for slightly different detection efficiencies and inverting the curve to present the depletion we achieve a very good agreement with the experimental data as can be seen in Fig. 5, where the resulting curve is plotted as a black line.

4 Discussion

We now proceed to discussing our experimental results in the context of the literature available on highly excited benzene cations. It is well established that photoionisation of benzene in the range of XUV photon energies above 15 eV has a quantum yield close to 1, whereas double ionisation is improbable under the conditions of the present experiment.[21,22] Therefore the time-dependent signals observed for the dication channels can be attributed to secondary ionisation by the VIS/NIR pulse. The transients thus show dynamics in the cationic states excited by the XUV pulse. For photon energies above 12 eV absorption of an XUV photon leads to photoemission from multiple electronic states.[22,24] The relevant electronic states of the cation were previously investigated by *ab initio* methods, in particular ADC(3) calculations which account for multi-electronic effects in the photoionisation.[25,26] These theoretical results are presented in Fig. 6, reproduced from ref. 26. The stick heights in the diagram correspond to single hole contributions to the electronic states of the cations. The first few cationic states have strong single orbital character as indicated by stick heights approaching 1. Above binding energies of 16 eV multi-electronic effects become predominant. The calculations predict the first satellite state (a state with multi-electronic character) at a binding energy of $E_b = 16.6$ eV, corresponding to the removal of one electron from the benzene molecule accompanied by the excitation of another electron from the HOMO to the LUMO. At binding energies $E_b \geq 18$ eV a breakdown of the molecular orbital picture is observed. Thus, ionisation out of the orbitals $2a_{1g}$, $2e_{1u}$ and $2e_{2g}$ no longer has a main transition with a strong contribution from single hole formation, but instead gives rise to groups of shake-up lines in the ionisation spectrum (*cf.* Fig. 6).

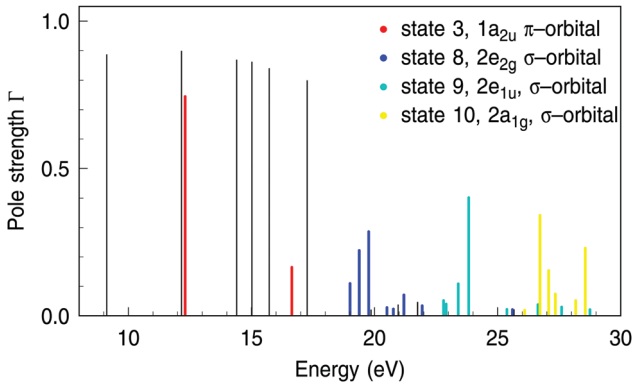

Fig. 6 Multi-electronic ionisation spectrum of C_6H_6 calculated with the ADC(3) method. The sticks correspond to electronic states of the benzene cation. The height of each stick gives the magnitude of a single hole contribution to the particular state. States with multi-electronic character are coloured and are labeled in the legend. The plot is reproduced from ref. 26.

In the experiment the XUV bandwidth in principle leads to the production of all cationic states shown in Fig. 6. However the relatively weak VIS/NIR probe intensities employed here favour ionisation with only few photons, restricting the probe ionisation to electronic states lying close to the double ionisation threshold of 24.9 eV. Indeed, in the experiments reported in ref. 15 performed with a constrained XUV bandwidth of 12–16 eV, no time-dependent dynamics was observed for the $C_6H_6^{2+}$ ion. Therefore, electronic states with a binding energy lower than 16 eV do not contribute to the experimental results reported in Fig. 3 and 4. Furthermore, the 1h states above 16 eV and the $1a_{2u}$ – satellite at 16.6 eV would require absorption of 5–6 VIS/NIR photons ($\hbar\omega$ = 1.65 eV) to create the dication and 7–8 photons to access the fragmentation channel leading to CH_3^+, which is improbable for the VIS/NIR intensities employed here. Therefore we interpret the dynamical behaviour as originating from the multi-electronic states with $E_b \geq 18$ eV.

This conclusion is supported by the depletion of the $C_4H_3^+$ fragment, shown in Fig. 5, which correlates with the time-dependent rise of the dication and the CH_3^+ fragment. It is known that the $C_4H_3^+$ fragment has an appearance energy of 17.5 eV.[18] Above 17.5 eV, the abundance rises in two steps which roughly correspond in energy to the positions of the $2e_{2g}$ and $2e_{1u}$ groups of states in Fig. 6 located at 19 eV and 23 eV, respectively. It is thus reasonable to assume that the signal in this fragmentation channel can serve as a proxy to the population of these two groups of states. Since $C_4H_3^+$ is the only fragment for which significant depletion is observed in our experiment, we suggest that the VIS/NIR pulse at small time delays mostly probes the $2e_{2g}$ and $2e_{1u}$ multi-electronic states leading to the enhancement of the dication signals and the depletion of the $C_4H_3^+$ fragment signal.

Our interpretation of the results shown in Fig. 3 and 4 is similar to our explanation for the XUV-NIR two-colour time dependence of dication formation in PAH molecules.[13] With increasing XUV-VIS/NIR delay, relaxation processes *via* conical intersections prohibit further ionisation by the probe pulse. For the lowest five states of the benzene cation (<16 eV) the dynamics have been subject to extensive theoretical and experimental investigations.[14,15,27,28] These states are low enough in energy such that only one-hole states are relevant. Ultrafast internal conversion processes were found to take place on timescales of $\tau \approx 10$ fs. For energies above 16 eV potential energy surfaces and conical intersections have not been investigated so far. However, the relaxation times of $\tau \approx 20$ fs observed in $C_6H_6^{2+}$ and CH_3^+ indicate that the topology of the intersecting potential energy surfaces for the multi-electronic states is very similar to that of the lower states, leading to rapid nonadiabatic relaxation on a comparable timescale. Previous experiments on small PAHs showed that the decay of the multi-electronic states depends on the number of aromatic rings.[13] The most rapid lifetime was observed for the smallest PAH naphthalene (τ = 29 fs). Due to strong similarities in the geometrical and in particular electronic structure, benzene can be expected to undergo relaxation processes similar to PAHs. The short lifetimes determined for benzene support this size-dependent trend.

The dynamics observed for the CH_3^+ fragment ions poses more challenges for interpretation. These fragments are created in a unimolecular dissociation process of the dication, when sufficient internal energy is available to overcome the barrier for this reaction.[29] The formation of CH_3^+ requires migration of two hydrogen atoms and multiple C–C bond cleavages. As seen in Fig. 2(c) for the partially deuterated benzene the fragments occur in all possible configurations, *i.e.* as CH_3^+, CH_2D^+, CHD_2^+ and CD_3^+. This shows that multiple routes to the formation of this fragment exist, which involve the exchange of protons between different carbon sites. The mechanisms proposed so far all describe a single, specific fragmentation pathway involving ring opening followed by migration of the two nearest protons to the end of the chain and abstraction of the CH_3^+ ion.[29,30] Based on our observations this mechanism cannot fully explain the dissociation reaction. For the proposed pathway no CH_3^+ and CD_3^+ should be observed for the partially deuterated benzene. However, in our experiments the intensity is distributed among all four fragments (*cf.* Fig. 2(c)) and is closer to a statistical distribution, which is expected to be 1 : 3 : 3 : 1 as calculated from the rotational symmetry numbers[31] assuming D_{3h} symmetry for the planar CH_3^+ and CD_3^+ ions and C_{2v} symmetry for the mixed ions, which also have a planar geometry. This observation suggests that in the fragmentation process the molecule undergoes proton scrambling, *i.e.* that protons may change sites several times before the fragmentation reaction is complete.

The two models (delayed exponential and two-exponential) applied to describe the transient behavior of this fragment suggest two different interpretations of the dynamics, neither of which can be preferred at the moment. The delayed exponential model can correspond to a propagation of the nuclear wavepacket from the Franck–Condon region towards a position on the multidimensional potential energy surface where relaxation occurs more efficiently. On the other hand, in the rise–decay model the rise time of Δt = 7 fs can represent relaxation from the initially

excited electronic state to a state from which probe laser ionisation – eventually leading to the production of CH_3^+ fragments – is more probable. In both models, at longer times further nonadiabatic relaxation to the ground state prohibits probe laser ionisation and gives rise to the decay part τ of the rise–decay function. Regardless of the choice between the two interpretations, a process on a timescale of $\approx$10 fs opens up the path to more efficient ionisation to electronic states in the dication that lead to subsequent proton migration and fragmentation of the dication.

5 Conclusions

In conclusion, we have performed an XUV-VIS/NIR pump–probe experiment with sub-10 fs temporal resolution to investigate the relaxation dynamics of excited cationic states of benzene, in particular highly excited states whose formation involves shake-up ionisation. The cationic states created by the XUV pulses are observed to decay rapidly *via* nonadiabatic relaxation on timescales of $<$20 fs. Experiments with varying XUV bandwidth as well as the observation of depletion in the $C_4H_3^+$ fragment in the presence of the probe VIS/NIR pulse allow us to assign the observed dynamics to the $2e_{2g}$ and $2e_{1u}$ groups of states, which have strong multi-electronic character. The timescales of non-adiabatic relaxation for these highly excited states are however similar to those observed and predicted for the lower lying cationic states,[15] suggesting that the relaxation is governed by a similar topology of intersecting potential energy surfaces.

Experiments conducted with partially deuterated benzene show that several pathways exist in the dication fragmentation leading to the CH_3^+ fragment, which indicate fast proton migration in the dissociation process. The CH_3^+ fragment channel also exhibits a non-trivial transient behavior, which can be described by two alternative models leading to different interpretations. One model with a delayed exponential decay suggests propagation of the nuclear wavepacket excited by the XUV pulse in search of the location in the multidimensional landscape of potential energy surfaces, where electronic relaxation is enhanced. The second rise–decay model suggests electronic relaxation from the initial to an intermediate state with a higher probe laser ionisation propensity from the latter. Further experimental and theoretical efforts are required to make the distinction between these two models.

Acknowledgements

F. L. and A. M. would like to thank ANR CIRCE CE30142716. G. R. thanks the Netherlands Organisation for Scientific Research (NWO) for financial support (Rubicon 68-50-1410).

References

1 C. Alcaraz, I. Fischer and D. Schröder, *Radical Chemistry in the Gas Phase*, John Wiley & Sons, Ltd, 2012.
2 A. G. G. M. Tielens, *Rev. Mod. Phys.*, 2013, **85**, 1021–1081.
3 L. S. Cederbaum, W. Domcke, J. Schirmer and W. V. Niessen, *Correlation Effects in the Ionization of Molecules: Breakdown of the Molecular Orbital Picture*, John Wiley & Sons, Inc., 2007, pp. 115–159.
4 W. Domcke and D. R. Yarkony, *Annu. Rev. Phys. Chem.*, 2012, **63**, 325–352.
5 A. Golan, K. B. Bravaya, R. Kudirka, O. Kostko, S. R. Leone, A. I. Krylov and M. Ahmed, *Nat. Chem.*, 2012, **4**, 323–329.
6 A. H. Zewail, *J. Phys. Chem. A*, 2000, **104**, 5660–5694.
7 A. Stolow, A. E. Bragg and D. M. Neumark, *Chem. Rev.*, 2004, **104**, 1719–1758.
8 E. Gagnon, P. Ranitovic, X.-M. Tong, C. L. Cocke, M. M. Murnane, H. C. Kapteyn and A. S. Sandhu, *Science*, 2007, **317**, 1374–1378.
9 M. Eckstein, C.-H. Yang, M. Kubin, F. Frassetto, L. Poletto, H.-H. Ritze, M. J. J. Vrakking and O. Kornilov, *J. Phys. Chem. Lett.*, 2015, **6**, 419–425.
10 H. Timmers, N. Shivaram and A. Sandhu, *Phys. Rev. Lett.*, 2012, **109**, 173001.
11 X. Zhou, P. Ranitovic, C. W. Hogle, J. H. D. Eland, H. C. Kapteyn and M. M. Murnane, *Nat. Phys.*, 2012, **8**, 232–237.
12 F. Calegari, D. Ayuso, A. Trabattoni, L. Belshaw, S. De Camillis, S. Anumula, F. Frassetto, L. Poletto, A. Palacios, P. Decleva, J. B. Greenwood, F. Martn and M. Nisoli, *Science*, 2014, **346**, 336–339.
13 A. Marciniak, V. Despré, T. Barillot, A. Rouzée, M. Galbraith, J. Klei, C.-H. Yang, C. Smeenk, V. Loriot, S. N. Reddy, A. Tielens, S. Mahapatra, A. I. Kuleff, M. Vrakking and F. Lépine, *Nat. Commun.*, 2015, **6**, 7909.
14 I. Bâldea and H. Köppel, *J. Chem. Phys.*, 2006, **124**, 064101.
15 M. C. E. Galbraith, S. Scheit, N. V. Golubev, G. Reitsma, N. Zhavoronkov, V. Despré, F. Lépine, A. I. Kuleff, M. J. J. Vrakking, O. Kornilov, H. Köppel and J. Mikosch, under review.
16 A. T. J. B. Eppink and D. H. Parker, *Rev. Sci. Instrum.*, 1997, **68**, 3477–3484.
17 O. Ghafur, W. Siu, P. Johnsson, M. F. Kling, M. Drescher and M. J. J. Vrakking, *Rev. Sci. Instrum.*, 2009, **80**, 033110.
18 D. Holland, D. Shaw, I. Sumner, M. Bowler, R. Mackie, L. Shpinkova, L. Cooper, E. Rennie, J. Parker and C. Johnson, *Int. J. Mass Spectrom.*, 2002, **220**, 31–51.
19 M. Alagia, P. Candori, S. Falcinelli, F. Pirani, M. S. P. Mundim, R. Richter, M. Rosi, S. Stranges and F. Vecchiocattivi, *Phys. Chem. Chem. Phys.*, 2011, **13**, 8245–8250.
20 H. M. Rosenstock, J. Dannacher and J. F. Liebman, *Radiat. Phys. Chem.*, 1982, **20**, 7–28.
21 T. Hartman, P. N. Juranić, K. Collins, B. Reilly, N. Appathurai and R. Wehlitz, *Phys. Rev. Lett.*, 2012, **108**, 023001.
22 E. Rennie, C. Johnson, J. Parker, D. Holland, D. Shaw and M. Hayes, *Chem. Phys.*, 1998, **229**, 107–123.
23 T. Suzuki, *Int. Rev. Phys. Chem.*, 2012, **31**, 265–318.
24 P. Baltzer, L. Karlsson, B. Wannberg, G. Öhrwall, D. M. P. Holland, M. A. MacDonald, M. A. Hayes and W. von Niessen, *Chem. Phys.*, 1997, **224**, 95–119.

25 L. S. Cederbaum, W. Domcke, J. Schirmer, W. von Niessen, G. H. F. Diercksen and W. P. Kraemer, *J. Chem. Phys.*, 1978, **69**, 1591–1603.
26 M. S. Deleuze, A. B. Trofimov and L. S. Cederbaum, *J. Chem. Phys.*, 2001, **115**, 5859–5882.
27 M. Döscher, H. Köppel and P. G. Szalay, *J. Chem. Phys.*, 2002, **117**, 2645–2656.
28 H. Köppel, M. Döscher, I. Bâldea, H.-D. Meyer and P. G. Szalay, *J. Chem. Phys.*, 2002, **117**, 2657–2671.
29 M. Alagia, P. Candori, S. Falcinelli, M. S. P. Mundim, F. Pirani, R. Richter, M. Rosi, S. Stranges and F. Vecchiocattivi, *J. Chem. Phys.*, 2011, **135**, 144304.
30 S. Anand and H. B. Schlegel, *J. Phys. Chem. A*, 2005, **109**, 11551–11559.
31 A. Fernández-Ramos, B. A. Ellingson, R. Meana-Pañeda, J. M. C. Marques and D. G. Truhlar, *Theor. Chem. Acc.*, 2007, **118**, 813–826.